

Available online at www.sciencedirect.com

ScienceDirect

www.elsevier.com/locate/jes

JES
JOURNAL OF
ENVIRONMENTAL
SCIENCES
www.jesc.ac.cn

Effects of NO₂ and SO₂ on the secondary organic aerosol formation from beta-pinene photooxidation

Xiangyu Zang^{1,2,3}, Zhaoyan Zhang^{2,3}, Yingqi Zhao^{2,3}, Gang Li², Hua Xie², Weiqing Zhang², Guorong Wu², Xueming Yang^{1,2,3,4}, Ling Jiang^{2,*}

¹Zhang Dayu School of Chemistry, Dalian University of Technology, Dalian 116024, China

²State Key Laboratory of Molecular Reaction Dynamics, Dalian Institute of Chemical Physics, Chinese Academy of Sciences, Dalian 116023, China

³University of Chinese Academy of Sciences, Beijing 100049, China

⁴Department of Chemistry, School of Science, Southern University of Science and Technology, Shenzhen 518055, China

ARTICLE INFO

Article history:

Received 30 July 2022

Revised 21 October 2022

Accepted 22 October 2022

Available online 1 November 2022

Keywords:

Secondary organic aerosol
Volatile organic compound
Anthropogenic pollutant
Beta-pinene
Photooxidation

ABSTRACT

Elucidating the effects of anthropogenic pollutants on the photooxidation of biogenic volatile organic compounds is crucial to understanding the fundamental mechanisms of secondary organic aerosol (SOA) formation. Here, the impacts of NO₂ and SO₂ on SOA formation from the photooxidation of a representative monoterpene, β-pinene, were investigated by a number of laboratory studies. The results indicated NO₂ enhanced the SOA mass concentrations and particle number concentrations under both low and high β-pinene conditions. This could be rationalized that the increased O₃ concentrations upon the NO_x photolysis was helpful for the generation of more amounts of O₃-oxidized products, which accelerated the SOA nucleation and growth. Combing with NO₂, the promotion of the SOA yield by SO₂ was mainly reflected in the increase of mass concentration, which might be due to the elimination of the newly formed particles by the initially formed particles. The observed low oxidation degree of SOA might be attributed to the fast growth of SOA, resulting in the uptake of less oxygenated gas-phase species onto the particle phase. The present findings have important implications for SOA formation affected by anthropogenic-biogenic interactions in the ambient atmosphere.

© 2023 The Research Center for Eco-Environmental Sciences, Chinese Academy of Sciences. Published by Elsevier B.V.

Introduction

Atmospheric aerosol plays an essential role in the Earth-atmosphere system because it provides condensation nuclei for cloud droplets and absorbs/scatters solar radiation

(Andreae and Crutzen, 1997; Novakov and Penner, 1993). Atmospheric aerosol has profound impacts on the atmospheric chemistry and air quality, climate, ecosystem, and public health (Hallquist et al., 2009; Moise et al., 2015; Shrivastava et al., 2017). Organic aerosol (OA) significantly contributes (20%–90%) to the submicron aerosol (Kanakidou et al., 2005; Murphy et al., 2006; Zhang et al., 2007), in which secondary organic aerosol (SOA) accounts for a large fraction of organic aerosol (Jimenez et al., 2009; Zhang et al., 2007).

* Corresponding author.

E-mail: ljjiang@dicp.ac.cn (L. Jiang).

For instance, the contribution of SOA to OA was 44%–71% for the severe haze pollution event in China during January 2013 (Huang et al., 2014).

The estimated emission of biogenic volatile organic compounds (BVOCs) is about 10 times higher than that of anthropogenic volatile organic compounds (AVOCs) (Guenther et al., 1995, 2012; Sindelarova et al., 2014). Among the BVOCs, the monoterpenes are important contributors to SOA because of their high emission rates, high reactivity, and relatively high SOA yields as compared to isoprene (Guenther et al., 1995; 2012). The reactions of BVOCs with anthropogenic pollutants (NO_x , SO_2 , OH, O_3 , etc.) are the major sources of the SOA formation (Atkinson and Arey, 2003). NO_x was proposed to affect the fate of the peroxy radical ($\text{RO}_2\cdot$) formed in the VOC oxidation, resulting in the change of reaction product distribution and SOA formation. SO_2 was suggested to play an important role in increasing the SOA yields via the influence of acidic aerosol or the direct uptake of biogenic hydrocarbons onto acidic aerosol (Kleindienst et al., 2006). The anthropogenic–biogenic interactions during SOA formation are more complex than their current representation in models, which might induce the uncertainties in the predicted SOA budget (Shrivastava et al., 2017). Therefore, elucidating the effects of anthropogenic pollutants on BVOC photooxidation is essential in establishing predictive SOA formation networks and improving air quality and climate simulations (Xu et al., 2015).

β -pinene accounts for 17% of the monoterpenes, with estimated emission of 18.9 Tg/year (Guenther et al., 2012). Chamber measurements of SOA formation in the $\text{NO}_3 + \beta$ -pinene reaction identified a series of organic nitrate species (Boyd et al., 2015; Fry et al., 2009; Shen et al., 2021). The investigation of the influence of NO_x on the β -pinene photooxidation indicated that NO_x enhanced the SOA yield at low NO_x concentrations ($[\text{NO}_x]$), whereas NO_x suppressed the SOA yield at high NO_x concentrations (Sarrafzadeh et al., 2016). Aerosol yield was found to be largely enhanced by more than 330% by NO_2 when the ratio of inorganic gases to β -pinene ranged from 0 to 1.3 (Xu et al., 2021). Recent studies on SOA formation from photooxidation of α -pinene and limonene showed that SO_2 induced nucleation and enhanced SOA mass formation (Zhao et al., 2018). It can be inferred that the effect of SO_2 on the SOA formation is rather clear as compared with the debated conclusions of NO_x . Yet, the studies on the combined effects of NO_x and SO_2 on the β -pinene photooxidation remain scarce. Note that NO was dominated in the composition of NO_x in previous experiments. Here, we investigated the individual effect of NO_2 and the combined effect of NO_2 and SO_2 on SOA formation from the β -pinene photooxidation. The NO_2 and SO_2 impacts on the SOA mass concentrations, particle number concentrations, and chemical compositions were uncovered by tuning the concentrations of NO_2 , SO_2 , and β -pinene ($[\text{NO}_2]$, $[\text{SO}_2]$, and $[\beta\text{-pinene}]$).

1. Materials and methods

The experiments were performed using a home-built aerosol apparatus described in detail previously (Zang et al., 2022) and briefly summarized below. The DICP-CAS chamber (Dalian Institute of Chemical Physics, Chinese Academy Sciences) had

a volume of 2 m^3 , which was made of fluorinated ethylene propylene film and set up in a temperature- and humidity-controlled housing. The DICP-CAS chamber was equipped with 40 black lights (GE F40BLB (40 W, 300–550 nm), General Electric Company, USA) to simulate the solar light spectrum (290–400 nm). The reactants in the chamber were well mixed with a fan.

The concentrations of NO , NO_2 , and NO_x were measured by a gas analyzer (Model 42i, Thermo Fisher Scientific, UK), those of SO_2 by a gas analyzer (Model 43i, Thermo Fisher Scientific, UK), and those of O_3 ($[\text{O}_3]$) by a gas analyzer (Model 49i, Thermo Fisher Scientific, UK), respectively. The VOCs were characterized by proton-transfer reaction mass spectrometer (PTR-QMS 3000, East & West Analytical Instruments, China). The number concentrations and size distributions of particles were measured by a scanning mobility particle sizer spectrometer (SMPS 3938NL76, TSI Incorporated, USA). The chemical compositions of particles were detected by a home-built aerosol time-of-flight mass spectrometer based on thermal desorption and electron ionization.

The wall loss rates of NO , NO_2 , and O_3 were 4.09×10^{-4} , 4.06×10^{-4} , and $7.42 \times 10^{-4} \text{ min}^{-1}$, respectively, consistent with the reported values of other chamber facilities (Bin Babar et al., 2016; Smith et al., 2019; Wang et al., 2014; Wu et al., 2007). The photolysis rate constant of NO_2 was evaluated to be 0.197 min^{-1} , which was comparable to that of the GIG-CAS chamber (Guangzhou Institute of Geochemistry, Chinese Academy Sciences, 0.206 min^{-1}) (Wang et al., 2014), the AIOFM-CAS chamber (Anhui Institute of Optics and Fine Mechanics, Chinese Academy Sciences, 0.210 min^{-1}) (Hu et al., 2014), and the Tsinghua chamber (0.230 min^{-1}) (Wu et al., 2007). The aerosol mass losses on smog chamber walls were corrected by the method as described in Pathak et al. (2007).

The liquid β -pinene (Aladdin, 99%) was introduced to the smog chamber by injecting it into the airline. The SOA formation from the β -pinene photooxidation was investigated at different concentrations (β -pinene: 320–2282 ppbV; NO_2 : 81–847 ppbV; SO_2 : 70–403 ppbV). The temperature in the chamber was around $296 \pm 1 \text{ K}$, and relative humidity was around 2%. All the present experiments were carried out without adding seed aerosol.

2. Results and discussion

2.1. Classification of β -pinene photooxidation stages

Under low or high concentrations of β -pinene, the individual effects of NO_2 on SOA formation were studied at different NO_2 levels. Then, the combined effects of NO_2 and SO_2 on SOA formation from the β -pinene photooxidation were explored by varying the concentration and injection time of SO_2 . The experimental conditions are overviewed in Tables 1 and 2. The initial NO_2 concentrations were slightly higher than the urban air during severe haze events (100–200 ppbV) (Bryant et al., 2020; Guo et al., 2020; Ma et al., 2021). The temporal development of the concentrations of NO , NO_2 , O_3 , β -pinene, and SOA during the photooxidation under low and high β -pinene conditions is shown in Fig. 1 and Appendix A Fig. S1, re-

Table 1 – Overview of the experimental conditions.

	$[\beta\text{-pinene}]_0$ (ppbV)	$[\text{NO}_x]_0$ (ppbV)	$[\text{NO}_2]_0$ (ppbV)	$[\text{SO}_2]_0$ (ppbV)	$[\beta\text{-pinene}]/$ $[\text{NO}_x]$	$[\text{O}_3]_{\max}$ (ppbV)	ΔROG (ppbV)	ΔM ($\mu\text{g}/\text{m}^3$)	SOA Yield (%)
Low β -pinene without SO_2	320	82	81	0	3.90	68	260	276.5	18.93
without SO_2 added	353	120	119	0	2.94	75	302	381.5	22.48
added	341	165	164	0	2.07	85	300	488.4	28.93
High β -pinene without SO_2	332	280	275	0	1.19	89	315	647.7	36.58
without SO_2 added	2146	628	625	0	3.4	407	1855	2492	23.90
High β -pinene with SO_2 added	1902	234	233	0	8.1	235	1271	1180	16.52
added	1904	851	847	0	2.2	337	1689	2608	27.48
2186	149	148	0	14.7	184	1475	900	10.86	
High β -pinene with SO_2 added	2058	146	145	70	14.2	259	1572	1521	17.21
2168	142	141	257	15.3	222	1522	1736.2	20.30	
2282	125	119	403	18.3	113	1384	1661.8	21.37	

$[X]_0$: the initial concentration of the species X; $[\text{O}_3]_{\max}$: the maximum mass concentration of O_3 ; ΔROG : the amount of reacted organic gas; ΔM : the mass concentration of formed SOA.

Table 2 – Experimental conditions as a function of the SO_2 injection time.

SO_2 injection time (hr)	$[\beta\text{-pinene}]_0$ (ppbV)	$[\text{NO}_x]_0$ (ppbV)	$[\text{NO}_2]_0$ (ppbV)	$[\text{SO}_2]_0$ (ppbV)	$[\beta\text{-pinene}]/$ $[\text{NO}_x]$	ΔROG (ppbV)	ΔM ($\mu\text{g}/\text{m}^3$)	SOA yield (%)
0	288	246	242	0	1.17	250	506.4	36.07
0	290	233	230	180	1.25	281	795.2	50.43
1	297	234	230	165	1.27	287	666.8	41.34
2	306	229	225	189	1.34	292	620.9	37.88

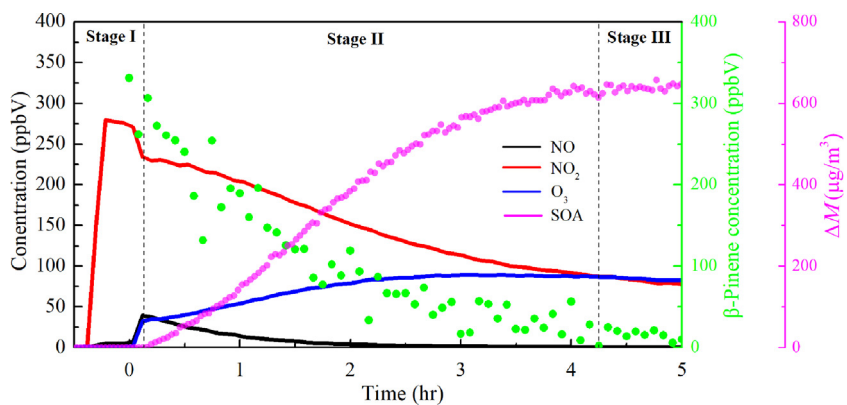


Fig. 1 – Temporal shape of the concentrations of NO, NO_2 , O_3 , β -pinene, and SOA during the photooxidation. The initial concentrations of β -pinene and NO_2 were 332 and 275 ppbV, respectively.

spectively. The β -pinene photooxidation could be classified to three stages as follows.

2.1.1. Stage I: Initial stage of photooxidation reaction

Upon NO_x photolysis, O_3 and OH^- were formed, which initialized the β -pinene photooxidation and generated the low volatile organic compounds. This stage had a short time duration and provided the prerequisite conditions for nucleation. The termination of stage I was marked by the maximization of NO concentration. The following reactions might be involved

in the stage I.





where $h\nu$ is the UV irradiation, M is the atmospheric trace gas, and $\text{O}(\text{P}^3)$ is the triplet oxygen.

2.1.2. Stage II: Nucleation and growth stage of SOA

As the reactions proceeded, the concentrations of NO and NO_2 decreased, whereas those of O_3 continuously increased and reached at a maximum value at this stage. The first- and second-generation products of β -pinene photooxidation reacted with the $\text{OH}\cdot$ radicals to produce abundant species, promoting the nucleation and growth of SOA. It was found that the time duration of stage II was related to the concentration of reactants. With the increase of the reactant concentrations, the capability of SOA nucleation was enhanced and the reactions were accelerated, and thus the time duration was shortened (Appendix A Fig. S1). The end of stage II was signed by the maximization of SOA yield.

The $\text{RO}_2\cdot$ radicals could react with NO to produce RONO_2 or $\text{RO}\cdot$ and NO_2 , resulting in the accumulation of O_3 . The $\text{OH}\cdot$ radicals could react with NO to generate HONO as temporary sinks. These reactions might lead to the decrease of NO concentrations. The decrease of NO_2 concentrations could be rationalized as follows. NO_2 might react with $\text{RO}_2\cdot$ to form RO_2NO_2 as temporary sinks and with $\text{OH}\cdot$ to generate HNO_3 . NO_2 might also loss on the particle surfaces or the chamber walls.

2.1.3. Stage III: aging stage of SOA

During this stage, the concentrations of NO, NO_2 , O_3 , and SOA were kept stably. The SOA oxidation started slowly, leading to an overall increase of the oxidation degree of SOA components. These findings were consistent with previous results that the newly-formed SOA were less oxidized and the highly oxidized compounds were detected after the atmospheric aging (Ng et al., 2010).

2.2. Effects of NO_2 on SOA mass concentration and particle number concentration

Fig. 2 shows the SOA yields, maximum O_3 concentrations, and mass concentrations of formed SOA under different conditions. It can be seen from Fig. 2a that in low β -pinene conditions, the SOA yield decreased with the increase of the VOC/ NO_x ratio, indicating that NO_x enhanced the SOA formation. This finding also held true for high β -pinene conditions (Fig. 2b). Our results were consistent with recent studies on the interaction between β -pinene and NO_2 , O_3 , SO_2 , and NH_3 under dark conditions (Xu et al., 2021). Previous investigation also suggested that the aerosol carbon yield from the β -pinene photooxidation depended strongly on the initial HC/ NO_x ratio (Pandis et al., 1991).

The SOA yield was positively correlated with the maximum O_3 concentrations. Fig. 2c, d, e, and f show that with the increase of the NO_x concentration, the maximum O_3 concentration increased and so did the mass concentration of

formed SOA, implying that the mass concentration of formed SOA could be relevant to the O_3 concentration. The formation of ozone in the reaction of β -pinene with NO_x is consistent with the empirical kinetic modeling approach (EKMA) curve (Kinosian, 1982), which might be reflected by the maximum O_3 concentration peaking at $\text{VOCs}/\text{NO}_x = 4$ as shown in Fig. 2d. It is reminiscent of recent observations that the mass peaks of SOA generated from the α -pinene- NO_2 photooxidation were similar to those produced from the α -pinene- O_3 system, evidencing the contribution of O_3 during the NO_2 photooxidation processes (Jia and Xu, 2020). The $\text{RO}_2\cdot + \text{RO}_2\cdot$ reaction usually produces the species with higher molecular weights (i.e., the monomer, dimer, and trimer of highly oxygenated molecules (HOMs)), which is assumed to take part in the new particle formation and the initial particle growth (Kirkby et al., 2016). The studies on the SOA formation from monoterpene oxidation suggested that the SOA nucleation was mainly suppressed by the $\text{RO}_2\cdot + \text{NO}$ reaction (Wildt et al., 2014; Zhao et al., 2018). In the previous experimental conditions with NO dominated in the NO_x system, the probability of the $\text{RO}_2\cdot + \text{NO}$ reaction was enhanced with the increase of NO_x concentration, leading to decline the $\text{RO}_2\cdot + \text{RO}_2\cdot$ reaction and reduce the SOA nucleation (Wildt et al., 2014; Zhao et al., 2018).

In the NO_x cycle induced by UV irradiation, NO and O_3 were accumulated to some extent when the β -pinene was not involved in the reactions, and the NO_x , NO, and O_3 concentrations tended to be stable. The $\text{RO}_2\cdot$ and $\text{HO}_2\cdot$ radicals formed upon UV irradiation would compete with O_3 in the reaction with NO, also resulting in the accumulation of O_3 . With the increase of O_3 concentrations, the β -pinene photooxidation was thus enhanced, resulting in the formation of more amounts of SOA.

The ozone production can also be described by the odd oxygen (the concentration of O_x is equivalent to the sum of $[\text{NO}_2]$ and $[\text{O}_3]$), which approximately represents the total oxygen concentration (Lu et al., 2010). The maximum O_x concentrations as a function of VOC/NO_x under low (a) and high (b) β -pinene conditions are shown in Appendix A Fig. S2, which were consistent with the trend of measured O_3 concentrations.

The SOA mass concentrations and particle size distributions with various NO_2 concentrations in low and high β -pinene conditions are shown in Fig. 3. It can be seen from Fig. 3a that the SOA mass concentration increased with the increase of the NO_2 concentration, implying that NO_2 improved the SOA nucleation during the β -pinene photooxidation. Furthermore, the mass concentrations of SOA formed in high β -pinene conditions were larger than those in low β -pinene conditions (Figs. 3a and b), suggesting that the SOA nucleation was also enhanced by increasing the β -pinene concentrations. This might account for the similar mass concentrations of SOA formed in the two conditions of 1904 ppbV β -pinene/847 ppbV NO_2 and 2146 ppbV β -pinene/625 ppbV NO_2 (Fig. 3b). Fig. 3c shows that in low β -pinene conditions, with the increase of the NO_2 concentration, the number concentrations of initial particles tended to increase and the particle sizes developed to be larger. In high β -pinene conditions (Fig. 3d), although the number concentrations of initial particles increased with increasing the NO_2 concentration, the particle sizes slightly changed with $[\text{NO}_2]$ below 847 ppbV;

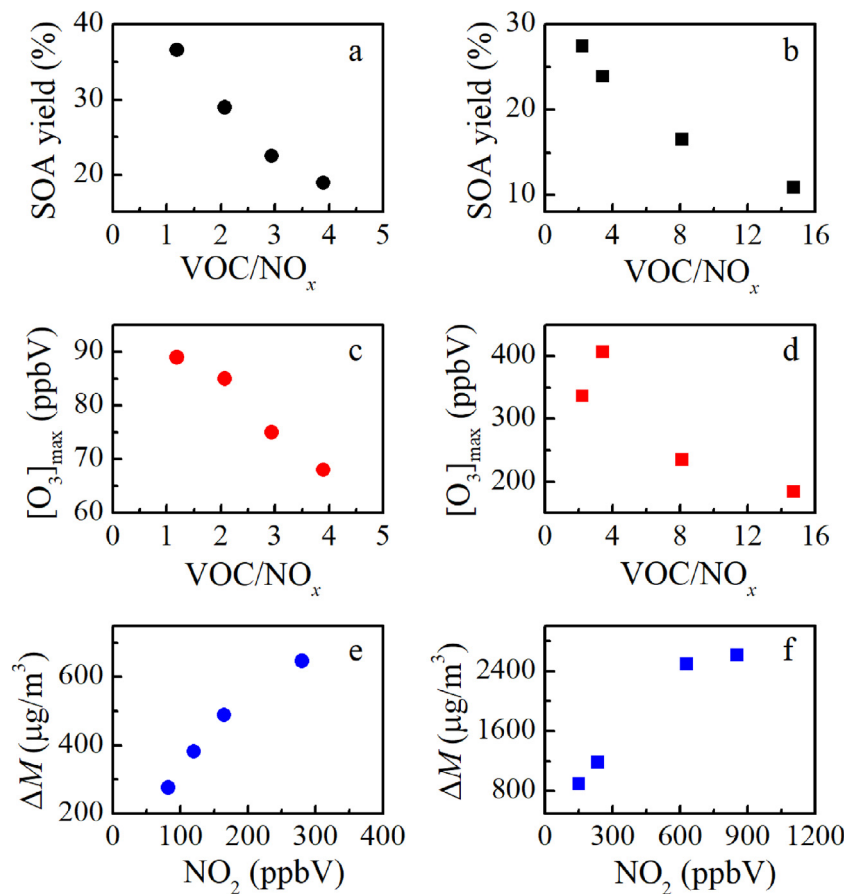


Fig. 2 – SOA yield as a function of VOC/NO_x under (a) low and (b) high β-pinene conditions. The maximum O₃ concentrations as a function of VOC/NO_x under (c) low and (d) high β-pinene conditions. The mass concentrations of formed SOA as a function of [NO₂] under (e) low and (f) high β-pinene conditions. The low and high β-pinene concentration was in the range of 320–353 and 1902–2168 ppbV, respectively.

with the increase of [NO₂] to 847 ppbV, the particle size distributions moved to a larger side. These observations might be relevant to the change of O₃ concentrations formed in different conditions. When [NO₂] was lower than 847 ppbV, the O₃/β-pinene ratios were relatively low, the O₃+β-pinene reaction generated a lot of the initial generation products with high volatility, making the particle size distributions nearly unchanged. When [NO₂] was increased to 847 ppbV, the increased [O₃] was helpful for the generation of more amounts of O₃-oxidized products, leading to the acceleration of the nucleation and growth of SOA.

2.3. Combining effects of NO₂ and SO₂ on SOA mass concentration and particle concentration

The oxidation of SO₂ to H₂SO₄ and subsequent condensation onto particles were proposed to play important roles in new particle formation (Brock et al., 2002). The acid-catalyzed heterogeneous reactions lead to a large increase in SOA production (Jang et al., 2002). SO₂ could react with Criegee intermediates formed from the alkene ozonolysis, affecting the ozonolysis mechanism of VOCs (Hung and Hoffmann, 2015;

Welz et al., 2012). It was also suggested that SO₂ could react with the peroxy radicals (RO₂[·]) in the gas phase (Kan et al., 1981), which reaction was too slow to compete with the sinks of RO₂[·] (Berndt et al., 2015). In highly polluted environments ([SO₂] > 40 ppbV), however, SO₂ could react with RO₂[·] at the aerosol surfaces, which particle-phase reaction rate ($\sim 10^{-13}$ cm³/(molecule·sec)) was 4 orders of magnitude larger than the value obtained for the gas-phase reaction ($\sim 10^{-17}$ cm³/(molecule·sec)) (Richards-Henderson et al., 2016; Sander and Watson, 1981).

It can be seen from Appendix A Fig. S3 shows that the SOA yields increased with the increase of the SO₂ concentrations, implying that SO₂ enhanced the SOA formation, which was consistent with previous studies on the effects of NO_x and SO₂ on the SOA formation from the photooxidation of α-pinene and limonene (Zhao et al., 2018). We also measured the SOA yield of β-pinene photooxidation with variation of SO₂ injection time (Fig. 4). The results indicated that the later the SO₂ injection time, the less the SOA yield. As compared to the experiments without SO₂, the SOA yield was still raised with the SO₂ injection at the latest time of 2 hr studied here. In particular, the increase of the SOA yield with the SO₂ injection at

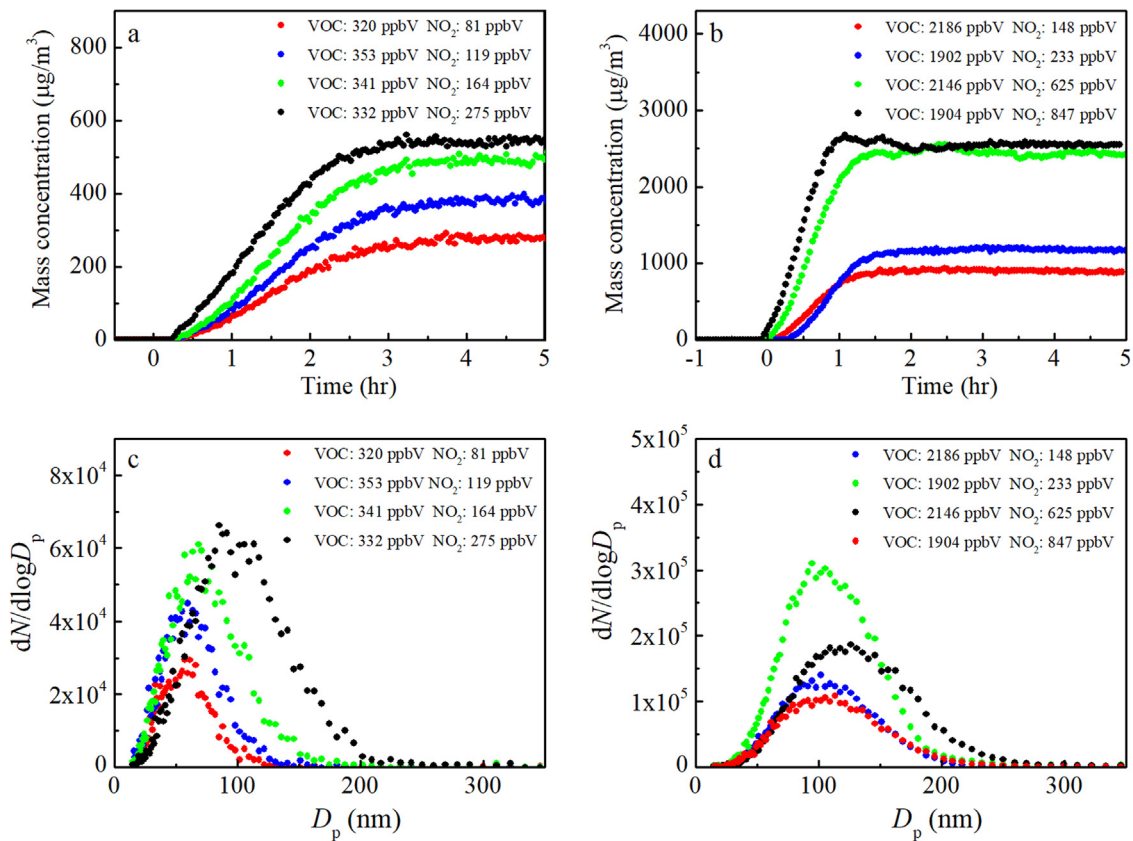


Fig. 3 – (a and b) SOA mass concentrations and (c and d) particle size distributions with various NO_2 concentrations in low and high β -pinene conditions. D_p : particle diameter; $dN/d\log D_p$: normalized number size distribution.

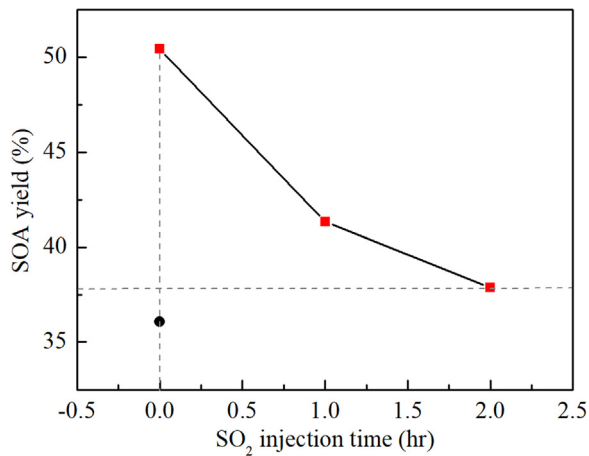


Fig. 4 – SOA yield as a function of SO_2 injection time in low β -pinene conditions. The detailed experimental conditions are listed in Table 2.

0 hr was much larger than that at 1 hr, indicating that the enhancement of SOA yield by SO_2 injected at the beginning of the reactions was larger than that by SO_2 injected during the reactions.

Such findings could be rationalized by the different roles of SO_2 in the influence of SOA formation mechanism. The

SO_2 oxidation induced the formation of new particles, providing more particle surfaces and volumes with the benefit for the VOC condensations and thus improving the nucleation (Zhao et al., 2018). The H_2SO_4 formed from SO_2 photooxidation could enhance the SOA formation via the acid-catalyzed heterogeneous reactions, which was assumed to be the primary pathway of SOA formation from the isoprene photooxidation (Lin et al., 2012; Surratt et al., 2007). SO_2 could react with the gas-phase organics (i.e., RO_2) to produce organic sulfates, which enhanced the aerosol nucleation (Hung and Hoffmann, 2015; Lightfoot et al., 1992).

It was found that the SOA mass concentration as a function of the SO_2 injection time (Fig. 5a) followed the trend of the SOA yield (Fig. 4), whereas the SOA particle concentration did not (Fig. 5b). This indicated that the enhancement of the SOA yield by SO_2 was mainly reflected in the increase of the SOA mass concentration. Fig. 5b showed that the SOA particle concentration with the SO_2 injection at 2 hr was close to that without the SO_2 injection, implying that the late injection of SO_2 during the nucleation reaction did not significantly induce the enhancement of the SOA particle concentration. This could be interpreted by the fact that the new particles produced by the SO_2 oxidation were eliminated via the condensations by the initial particles formed during the nucleation; SO_2 can be oxidized to H_2SO_4 and subsequently enhanced the uptake capability of the nuclei by acid catalysis. As a result, the extent for the change of the SOA mass concentration was

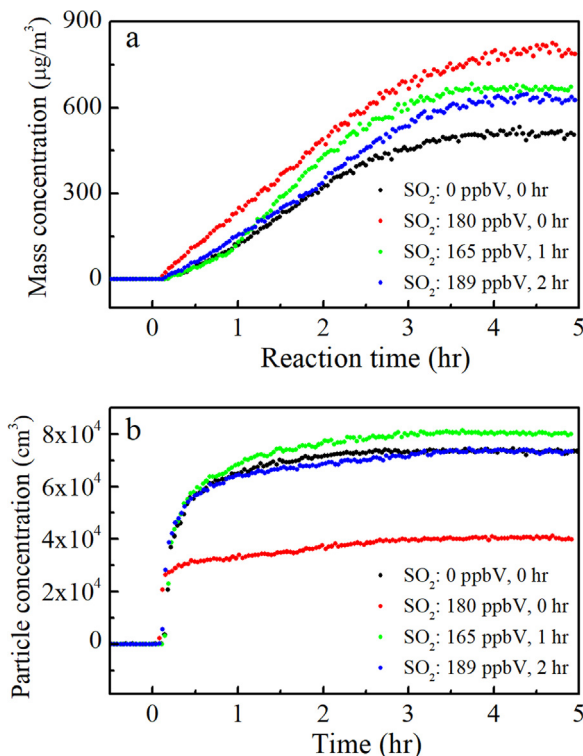


Fig. 5 – (a) SOA mass concentration and **(b)** particle concentration of β -pinene photooxidation without/with different SO_2 injection times. The experimental conditions are given in Table 2.

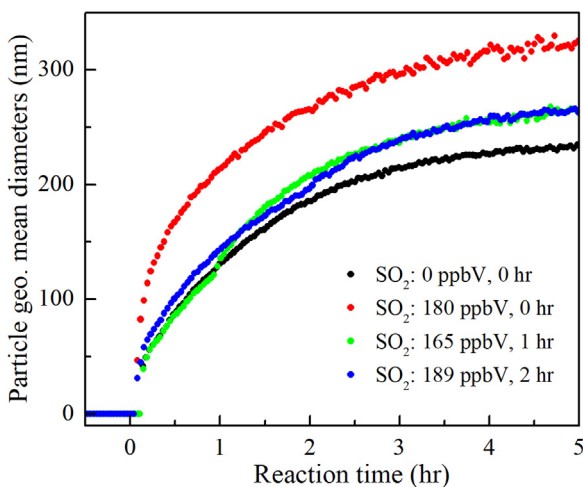


Fig. 6 – Geometric mean diameter of SOA of β -pinene photooxidation without/with different SO_2 injection times. The experimental conditions are given in Table 2.

visibly larger than that of the particle concentration. Such SO_2 effects were also demonstrated by the influence of the SO_2 injection time on the SOA geometric mean diameter (Fig. 6), with similarity to that on the SOA mass concentration (Fig. 5a). The geometric mean diameter of SOA with SO_2 injected at the beginning of the reactions (at 0 hr) was larger than that with SO_2 injected during the reactions (at 1 and 2 hr), implying that

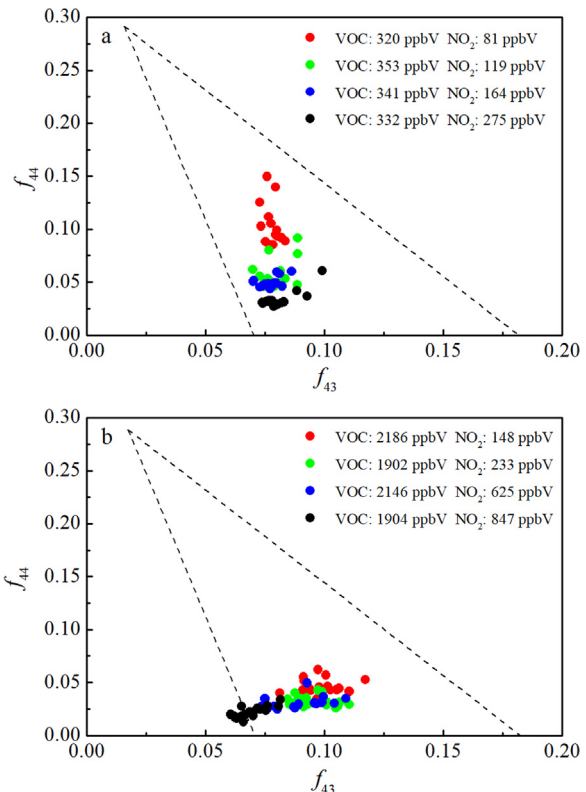


Fig. 7 – The f_{44} vs. f_{43} for all the SOA components formed from the β -pinene photooxidation in (a) low and (b) high β -pinene conditions. The “triangle” parameterization space where ambient OOA components fall (Ng et al., 2010) is represented by dash lines.

large amounts of organics were involved in the initial stages of the reactions, resulting in large yield and geometric mean diameter of SOA.

2.4. Effects of NO_2 on SOA chemical composition

Previous aerosol mass spectra showed that organic aerosol at most sites can be mainly classified into oxygenated organic aerosol (OOA) and hydrocarbon-like organic aerosol (HOA) (Zhang et al., 2007). OOA constitutes a substantial fraction ($72\% \pm 21\%$) of the total organic mass (Jimenez et al., 2009; Zhang et al., 2007). The subcomponents of OOA can be described as low-volatility OOA (LV-OOA) and semivolatile OOA (SV-OOA), which could be characterized by two main ions of m/z (ratio of mass to charge) = 44 (CO_2^+) and m/z 43 (mostly $\text{C}_2\text{H}_3\text{O}^+$) in the mass spectra (Chhabra et al., 2011; Ng et al., 2010). It has been demonstrated that the LV-OOA component spectra had higher f_{44} (ratio of m/z 44 to total signal) and lower f_{43} (ratio of m/z 43 to total signal) than SV-OOA (Ng et al., 2010). The average value of f_{44} was observed at 0.17 ± 0.04 for LV-OOA and 0.07 ± 0.04 for SV-OOA (Ng et al., 2010), respectively.

Fig. 7 shows the f_{44} vs. f_{43} values for all the SOA components formed from the β -pinene photooxidation in low and high β -pinene conditions. The SOA components were mainly concentrated in the lower half of the triangle, revealing a low

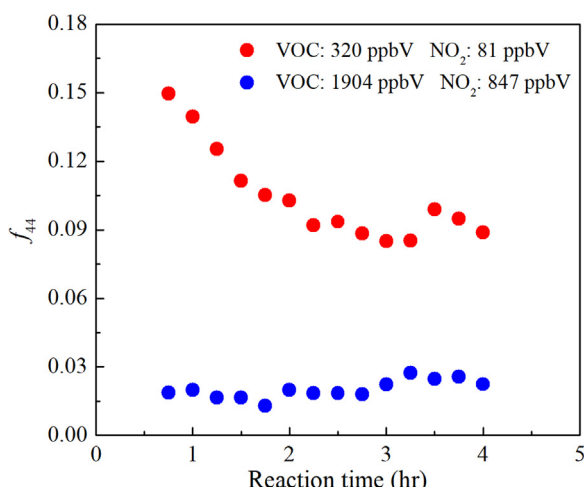


Fig. 8 – The f_{44} of all the SOA components formed from the β -pinene photooxidation as a function of reaction time under low (red dot) and high (blue dot) initial concentrations.

oxidation degree of SOA. It was speculated that the time duration from the SOA formation to the detection was fairly short because of the small smog chamber, and thus the SOA did not reach the oxidation degree as the field measurements. The LV-OOA and SV-OOA overlapped in the lower half of the triangle, suggesting a large variability of the chemical compositions.

In low β -pinene conditions, the f_{44} value decreased with increasing NO_x concentration, whereas the f_{43} value slightly changed (Fig. 7a). In high β -pinene conditions, the f_{43} value decreased with increasing NO_2 concentration, whereas the f_{44} value remained virtually unchanged (Fig. 7b). These findings might be attributed to the fast growth of SOA, resulting in the uptake of less oxygenated gas-phase species onto the particle phase and consequently a low f_{44} value. This phenomenon might also result from the ozone isopleth effect in the photochemical reaction between VOCs and NO_x (the EKMA curve) (Kinosian, 1982).

It can be seen from Fig. 8 that the f_{44} value (0.08–0.15) decreased with the reaction time under low initial concentration and slightly changed (~0.02) under high initial concentration. At the initial stage of SOA growth, the highly oxygenated LV-OOA readily partitioned into the particle phase. With the proceeding of the reactions, the highly oxygenated species were diluted by the less oxygenated SV-OOA, leading to a decline in the f_{44} value. This finding was consistent with the field observation of rapid particle growth induced by the semivolatile organic compounds (Zaveri et al., 2022). Previous studies indicated that highly-oxygenated low-volatility compounds were favorably formed under low initial precursor concentration and lowly-oxygenated high-volatility intermediate compounds were the major products under high initial precursor concentration (Alfarra et al., 2012; Chen et al., 2019). As a result, the f_{44} value at low initial concentration was larger than that at high initial concentration, supporting the present chamber measurements (Fig. 8).

3. Conclusions and implications

The effects of NO_2 and SO_2 on the SOA mass concentrations, particle number concentrations, and chemical compositions for the β -pinene photooxidation were investigated under different concentrations. The evolution of β -pinene photooxidation can be classified to three stages. In the first stage (initialization of photooxidation reaction), O_3 and OH^- were formed upon NO_x photolysis, which initialized the β -pinene photooxidation and generated the low volatile organic compounds. In the second stage (SOA nucleation and growth), the first- and second-generation products of β -pinene photooxidation reacted with various radicals (i.e., RO^- , RO_2^- , OH^-) to produce abundant species, promoting the nucleation and growth of SOA. In the third stage (SOA aging), the concentrations of NO , NO_2 , O_3 , and SOA were reasonably stable.

NO_2 promoted the SOA mass concentrations and particle number concentrations under both low and high β -pinene conditions, which were different from the suppression effects of NO_x on the SOA formation from photooxidation of α -pinene and limonene. In the NO_x cycle induced by UV irradiation, the increased O_3 concentrations helped to produce more amounts of O_3 -oxidized products during the β -pinene photooxidation under the present experimental conditions, which accelerated the nucleation and growth of SOA. The enhancement of the SOA yield by SO_2 was mainly reflected in the increase of the SOA mass concentration. The new particles produced by the SO_2 oxidation were feasibly eliminated via the condensations by the particles formed during the initial nucleation; SO_2 can be oxidized to H_2SO_4 and subsequently enhanced the uptake capability of the nuclei by acid catalysis. The observed low oxidation degree of SOA might be attributed to the fast growth of SOA, resulting in the uptake of less oxygenated gas-phase species onto the particle phase.

While β -pinene is an important contributor to anthropogenic volatile organic compounds, NO_2 and SO_2 are two vital anthropogenic pollutants and co-exist in the ambient atmosphere. The observed effects of NO_2 and SO_2 on the SOA mass concentration, particle concentration, and chemical compositions provide important information for fundamental understanding of the initial steps of β -pinene oxidation and the subsequent processes of new particle formation. The present findings have important implications for the assessment of SOA formation affected by biogenic-anthropogenic interactions and ultimate reduction of anthropogenic emissions.

Declaration of Competing Interest

The authors declare that they have no known competing financial interests or personal relationships that could have appeared to influence the work reported in this paper.

Acknowledgments

The authors gratefully acknowledge the Dalian Coherent Light Source (DCLS) for support and assistance. This work

was supported by the National Natural Science Foundation of China (Nos. 22125303, 92061203, and 22288201), the National Key Research and Development Program of China (No. 2021YFA1400501), Innovation Program for Quantum Science and Technology (No. 2021ZD0303304), Dalian Institute of Chemical Physics (No. DICP DCLS201702), Chinese Academy of Sciences (No. GJSTD20220001), and K. C. Wong Education Foundation (No. GJTD-2018-06).

Appendix A Supplementary data

Supplementary material associated with this article can be found in the online version at doi:[10.1016/j.jes.2022.10.040](https://doi.org/10.1016/j.jes.2022.10.040).

REFERENCES

- Alfarra, M.R., Hamilton, J.F., Wyche, K.P., Good, N., Ward, M.W., Carr, T., et al., 2012. The effect of photochemical ageing and initial precursor concentration on the composition and hygroscopic properties of beta-caryophyllene secondary organic aerosol. *Atmos. Chem. Phys.* 12, 6417–6436.
- Andreae, M.O., Crutzen, P.J., 1997. Atmospheric aerosols: Biogeochemical sources and role in atmospheric chemistry. *Science* 276, 1052–1058.
- Atkinson, R., Arey, J., 2003. Atmospheric degradation of volatile organic compounds. *Chem. Rev.* 103, 4605–4638.
- Berndt, T., Richters, S., Kaethner, R., Voigtlaender, J., Stratmann, F., Sipilae, M., et al., 2015. Gas-phase ozonolysis of cycloalkenes: formation of highly oxidized RO₂ radicals and their reactions with NO, NO₂, SO₂, and other RO₂ radicals. *J. Phys. Chem. A* 119, 10336–10348.
- Bin Babar, Z., Park, J.-H., Kang, J., Lim, H.-J., 2016. Characterization of a smog chamber for studying formation and physicochemical properties of secondary organic aerosol. *Aerosol Air Qual. Res.* 16, 3102–3113.
- Boyd, C.M., Sanchez, J., Xu, L., Eugene, A.J., Nah, T., Tuet, W.Y., et al., 2015. Secondary organic aerosol formation from the beta-pinene + NO₃ system: effect of humidity and peroxy radical fate. *Atmos. Chem. Phys.* 15, 7497–7522.
- Brock, C.A., Washenfelder, R.A., Trainer, M., Ryerson, T.B., Wilson, J.C., Reeves, J.M., et al., 2002. Particle growth in the plumes of coal-fired power plants. *J. Geophys. Res.-Atmos.* 107, 4155.
- Bryant, D.J., Dixon, W.J., Hopkins, J.R., Dunmore, R.E., Pereira, K., Shaw, M., et al., 2020. Strong anthropogenic control of secondary organic aerosol formation from isoprene in Beijing. *Atmos. Chem. Phys.* 20, 7531–7552.
- Chen, T., Liu, Y., Chu, B., Liu, C., Liu, J., Ge, Y., et al., 2019. Differences of the oxidation process and secondary organic aerosol formation at low and high precursor concentrations. *J. Environ. Sci.* 79, 256–263.
- Chhabra, P.S., Ng, N.L., Canagaratna, M.R., Corrigan, A.L., Russell, L.M., Worsnop, D.R., et al., 2011. Elemental composition and oxidation of chamber organic aerosol. *Atmos. Chem. Phys.* 11, 8827–8845.
- Fry, J.L., Kiendler-Scharr, A., Rollins, A.W., Wooldridge, P.J., Brown, S.S., Fuchs, H., et al., 2009. Organic nitrate and secondary organic aerosol yield from NO₃ oxidation of beta-pinene evaluated using a gas-phase kinetics/aerosol partitioning model. *Atmos. Chem. Phys.* 9, 1431–1449.
- Guenther, A., Hewitt, C.N., Erickson, D., Fall, R., Geron, C., Graedel, T., et al., 1995. A global model of natural volatile organic compound emissions. *J. Geophys. Res.-Atmos.* 100, 8873–8892.
- Guenther, A.B., Jiang, X., Heald, C.L., Sakulyanontvittaya, T., Duhl, T., Emmons, L.K., et al., 2012. The model of emissions of gases and aerosols from nature version 2.1 (MEGAN2.1): an extended and updated framework for modeling biogenic emissions. *Geosci. Model Dev.* 5, 1471–1492.
- Guo, S., Hu, M., Peng, J., Wu, Z., Zamora, M.L., Shang, D., et al., 2020. Remarkable nucleation and growth of ultrafine particles from vehicular exhaust. *Proc. Natl. Acad. Sci. USA* 117, 3427–3432.
- Hallquist, M., Wenger, J.C., Baltensperger, U., Rudich, Y., Simpson, D., Claeys, M., et al., 2009. The formation, properties and impact of secondary organic aerosol: current and emerging issues. *Atmos. Chem. Phys.* 9, 5155–5236.
- Hu, C.-j., Cheng, Y., Pan, G., Gai, Y.-b., Gu, X.-j., Zhao, W.-x., et al., 2014. A smog chamber facility for qualitative and quantitative study on atmospheric chemistry and secondary organic aerosol. *Chin. J. Chem. Phys.* 27, 631–639.
- Huang, R.-J., Zhang, Y., Bozzetti, C., Ho, K.-F., Cao, J.-J., Han, Y., et al., 2014. High secondary aerosol contribution to particulate pollution during haze events in China. *Nature* 514, 218–222.
- Hung, H.-M., Hoffmann, M.R., 2015. Oxidation of gas-phase SO₂ on the surfaces of acidic microdroplets: Implications for sulfate and sulfate radical anion formation in the atmospheric liquid phase. *Environ. Sci. Technol.* 49, 13768–13776.
- Jang, M.S., Czoschke, N.M., Lee, S., Kamens, R.M., 2002. Heterogeneous atmospheric aerosol production by acid-catalyzed particle-phase reactions. *Science* 298, 814–817.
- Jia, L., Xu, Y., 2020. The role of functional groups in the understanding of secondary organic aerosol formation mechanism from alpha-pinene. *Sci. Total Environ.* 738, 139831.
- Jimenez, J.L., Canagaratna, M.R., Donahue, N.M., Prevot, A.S.H., Zhang, Q., Kroll, J.H., et al., 2009. Evolution of organic aerosols in the atmosphere. *Science* 326, 1525–1529.
- Kan, C.S., Calvert, J.G., Shaw, J.H., 1981. Oxidation of sulfur dioxide by methylperoxy radicals. *J. Phys. Chem.* 85, 1126–1132.
- Kanakidou, M., Seinfeld, J.H., Pandis, S.N., Barnes, I., Dentener, F.J., Facchini, M.C., et al., 2005. Organic aerosol and global climate modelling: a review. *Atmos. Chem. Phys.* 5, 1053–1123.
- Kinosian, J.R., 1982. Ozone-precursor relationships from EKMA diagrams. *Environ. Sci. Technol.* 16, 880–883.
- Kirkby, J., Duplissy, J., Sengupta, K., Frege, C., Gordon, H., Williamson, C., et al., 2016. Ion-induced nucleation of pure biogenic particles. *Nature* 533, 521–526.
- Kleindinst, T.E., Edney, E.O., Lewandowski, M., Offenberg, J.H., Jaoui, M., 2006. Secondary organic carbon and aerosol yields from the irradiations of isoprene and alpha-pinene in the presence of NO_x and SO₂. *Environ. Sci. Technol.* 40, 3807–3812.
- Lightfoot, P.D., Cox, R.A., Crowley, J.N., Destriau, M., Hayman, G.D., Jenkin, M.E., et al., 1992. Organic peroxy radicals - kinetics, spectroscopy and tropospheric chemistry. *Atmos. Environ., Part A* 26, 1805–1961.
- Lin, Y.-H., Zhang, Z., Docherty, K.S., Zhang, H., Budisulistiorini, S.H., Rubitschun, C.L., et al., 2012. Isoprene epoxydiols as precursors to secondary organic aerosol formation: Acid-catalyzed reactive uptake studies with authentic compounds. *Environ. Sci. Technol.* 46, 250–258.
- Lu, K., Zhang, Y., Su, H., Brauers, T., Chou, C.C., Hofzumahaus, A., et al., 2010. Oxidant (O₃ + NO₂) production processes and formation regimes in Beijing. *J. Geophys. Res.-Atmos.* 115, D07303.
- Ma, P., Quan, J., Jia, X., Liao, Z., Wang, Q., Cheng, Z., et al., 2021. Effects of ozone and relative humidity in secondary inorganic aerosol formation during haze events in Beijing, China. *Atmos. Res.* 264, 105855.
- Moise, T., Flores, J.M., Rudich, Y., 2015. Optical properties of secondary organic aerosols and their changes by chemical processes. *Chem. Rev.* 115, 4400–4439.
- Murphy, D.M., Cziczo, D.J., Froyd, K.D., Hudson, P.K., Matthew, B.M., Middlebrook, A.M., et al., 2006. Single-particle mass

- spectrometry of tropospheric aerosol particles. *J. Geophys. Res.-Atmos.* 111, D23S32.
- Ng, N.L., Canagaratna, M.R., Zhang, Q., Jimenez, J.L., Tian, J., Ulbrich, I.M., et al., 2010. Organic aerosol components observed in Northern Hemispheric datasets from aerosol mass spectrometry. *Atmos. Chem. Phys.* 10, 4625–4641.
- Novakov, T., Penner, J.E., 1993. Large contribution of organic aerosols to cloud-condensation-nuclei concentrations. *Nature* 365, 823–826.
- Pandis, S.N., Paulson, S.E., Seinfeld, J.H., Flagan, R.C., 1991. Aerosol formation in the photooxidation of isoprene and beta-pinene. *Atmos. Environ., Part A* 25, 997–1008.
- Pathak, R.K., Stanier, C.O., Donahue, N.M., Pandis, S.N., 2007. Ozonolysis of alpha-pinene at atmospherically relevant concentrations: temperature dependence of aerosol mass fractions (yields). *J. Geophys. Res.-Atmos.* 112, D03201.
- Richards-Henderson, N.K., Goldstein, A.H., Wilson, K.R., 2016. Sulfur dioxide accelerates the heterogeneous oxidation rate of organic aerosol by hydroxyl radicals. *Environ. Sci. Technol.* 50, 3554–3561.
- Sander, S.P., Watson, R.T., 1981. A kinetics study of the reaction of SO₂ with CH₃O₂. *Chem. Phys. Lett.* 77, 473–475.
- Sarrafzadeh, M., Wildt, J., Pullinen, I., Springer, M., Kleist, E., Tillmann, R., et al., 2016. Impact of NO_x and OH on secondary organic aerosol formation from beta-pinene photooxidation. *Atmos. Chem. Phys.* 16, 11237–11248.
- Shen, H., Zhao, D., Pullinen, I., Kang, S., Vereecken, L., Fuchs, H., et al., 2021. Highly oxygenated organic nitrates formed from NO₃ radical-initiated oxidation of beta-pinene. *Environ. Sci. Technol.* 55, 15658–15671.
- Shrivastava, M., Cappa, C.D., Fan, J., Goldstein, A.H., Guenther, A.B., Jimenez, J.L., et al., 2017. Recent advances in understanding secondary organic aerosol: Implications for global climate forcing. *Rev. Geophys.* 55, 509–559.
- Sindelarova, K., Granier, C., Bouarar, I., Guenther, A., Tilmes, S., Stavrakou, T., et al., 2014. Global data set of biogenic VOC emissions calculated by the MEGAN model over the last 30 years. *Atmos. Chem. Phys.* 14, 9317–9341.
- Smith, D.M., Fiddler, M.N., Sexton, K.G., Bililign, S., 2019. Construction and characterization of an indoor smog chamber for measuring the optical and physicochemical properties of aging biomass burning aerosols. *Aerosol Air Qual. Res.* 19, 467–483.
- Surratt, J.D., Lewandowski, M., Offenberg, J.H., Jaoui, M., Kleindienst, T.E., Edney, E.O., et al., 2007. Effect of acidity on secondary organic aerosol formation from isoprene. *Environ. Sci. Technol.* 41, 5363–5369.
- Wang, X., Liu, T., Bernard, F., Ding, X., Wen, S., Zhang, Y., et al., 2014. Design and characterization of a smog chamber for studying gas-phase chemical mechanisms and aerosol formation. *Atmos. Meas. Tech.* 7, 301–313.
- Welz, O., Savee, J.D., Osborn, D.L., Vasu, S.S., Percival, C.J., Shallcross, D.E., et al., 2012. Direct kinetic measurements of Criegee intermediate (CH₂OO) formed by reaction of CH₂I with O₂. *Science* 335, 204–207.
- Wildt, J., Mentel, T.F., Kiendler-Scharr, A., Hoffmann, T., Andres, S., Ehn, M., et al., 2014. Suppression of new particle formation from monoterpene oxidation by NO_x. *Atmos. Chem. Phys.* 14, 2789–2804.
- Wu, S., Lu, Z., Hao, J., Zhao, Z., Li, J., Takekawa, H., et al., 2007. Construction and characterization of an atmospheric simulation smog chamber. *Adv. Atmos. Sci.* 24, 250–258.
- Xu, L., Yang, Z., Tsона, N.T., Wang, X., George, C., Du, L., 2021. Anthropogenic-biogenic interactions at night: enhanced formation of secondary aerosols and particulate nitrogen- and sulfur-containing organics from beta-pinene oxidation. *Environ. Sci. Technol.* 55, 7794–7807.
- Xu, L., Guo, H., Boyd, C.M., Klein, M., Bougiatioti, A., Cerully, K.M., et al., 2015. Effects of anthropogenic emissions on aerosol formation from isoprene and monoterpenes in the southeastern United States. *Proc. Natl. Acad. Sci. USA* 112, 37–42.
- Zang, X., Zhang, Z., Jiang, S., Zhao, Y., Wang, T., Wang, C., et al., 2022. Aerosol mass spectrometry of neutral species based on a tunable vacuum ultraviolet free electron laser. *Phys. Chem. Chem. Phys.* 24, 16484–16492.
- Zaveri, R.A., Wang, J., Fan, J., Zhang, Y., Shilling, J.E., Zelenyuk, A., et al., 2022. Rapid growth of anthropogenic organic nanoparticles greatly alters cloud life cycle in the Amazon rainforest. *Sci. Adv.* 8, eabj0329.
- Zhang, Q., Jimenez, J.L., Canagaratna, M.R., Allan, J.D., Coe, H., Ulbrich, I., et al., 2007. Ubiquity and dominance of oxygenated species in organic aerosols in anthropogenically-influenced Northern Hemisphere midlatitudes. *Geophys. Res. Lett.* 34, L13801.
- Zhao, D., Schmitt, S.H., Wang, M., Acir, I.-H., Tillmann, R., Tan, Z., et al., 2018. Effects of NO_x and SO₂ on the secondary organic aerosol formation from photooxidation of alpha-pinene and limonene. *Atmos. Chem. Phys.* 18, 1611–1628.